GEOPHYSICS, VOL. 69, NO. 1 (JANUARY-FEBRUARY 2004); P. 16–24, 8 FIGS.
10.1190/1.1649371

Case History

Crosswell seismic imaging in a contaminated basalt aquifer

Thomas M. Daley*, Ernest L. Majer*, and John E. Peterson*

ABSTRACT

Multiple seismic crosswell surveys have been acquired and analyzed in a fractured basalt aquifer at Idaho National Engineering and Environmental Laboratory. Most of these surveys used a high-frequency (1000–10,000 Hz) piezoelectric seismic source to obtain P-wave velocity tomograms. The P-wave velocities range from less than 3200 m/s to more than 5000 m/s. Additionally, a new type of borehole seismic source was deployed as part of the subsurface characterization program at this contaminated groundwater site. This source, known as an orbital vibrator, allows simultaneous acquisition of P- and S-waves at frequencies of 100 to 400 Hz, and acquisition over larger distances. The velocity tomograms show a relationship to contaminant transport in the groundwater; zones of high contaminant concentration are coincident with zones of low velocity and high attenuation and are interpreted to be fracture zones at the boundaries between basalt flows. The orbital vibrator data show high V_p/V_s values, from 1.8 to 2.8. In spite of the lower resolution of orbital vibrator data, these data were sufficient for constraining hydrologic models at this site while achieving imaging over large interwell distances. The combination of piezoelectric data for closer well spacing and orbital vibrator data for larger well spacings has provided optimal imaging capability and has been instrumental in our understanding of the site aquifer's hydrologic properties and its scale of heterogeneity.

INTRODUCTION

The remediation of contaminated aquifers is important to the long-term health of water supplies. The design of appropriate remediation strategies (such as bioremediation or pump-and-treat) requires an understanding of aquifer properties and of the subsurface structure that may affect those properties.

Seismology provides important methods for imaging subsurface structure and material properties. Seismic-reflection imaging, using surface sources and receivers, has been widely used to delineate structure; however, the resolution of subsurface features is limited by seismic wavelength and attenuation. The need for higher resolution imaging has led to borehole seismic techniques that place sources and sensors at depth in wells, closer to the target and beneath the highly attenuative surface layers. This approach uses the shorter wavelengths generated by borehole sources.

One important method for borehole seismology is crosswell tomography. Crosswell seismic surveys have been used for many years to tomographically image P-wave velocity between wells (Mason, 1981; Peterson et al., 1985). More recently, crosswell S-waves have also been used to map S-wave velocity (Harris et al., 1995), and both P- and S-wave crosswell reflectivities have been analyzed to delineate structural features (Rector et al., 1995). Seismic properties have been used to constrain hydrologic properties and contaminant transport in synthetic data studies (e.g., Rubin et al., 1992; Hyndman et al., 1994; Hubbard et al., 1999) and in field studies (e.g., McKenna and Poeter, 1995; Yamamoto et al., 1995; Hyndman and Gorelick, 1996). However, the majority of these shallow-aquifer studies focus on sedimentary environments. Few tomographic studies have been performed to characterize contaminated igneous environments.

As part of a U.S. Department of Energy research program (the Environmental Management Science Program), Lawrence Berkeley National Laboratory (LBNL) conducted crosswell seismic studies at the Idaho National Environmental and Engineering Laboratory (INEEL) in a fractured basalt aquifer (part of the Snake River Plain aquifer), which has been contaminated locally by waste disposal into a well at the Test Area North (TAN) site (Figure 1). Multiple crosswell surveys were acquired during two field sessions. The initial surveys

Manuscript received by the Editor December 7, 2001; revised manuscript received May 19, 2003.
*Center for Computational Seismology, Lawrence Berkeley National Laboratory, 1 Cyclotron Road, MS 90-1116, Berkeley, California 94720. E-mail: tmdaley@1bl.gov; elmajer@1bl.gov; jepeterson@1bl.gov.

used a piezoelectric source that provided high-frequency (1000–10,000 Hz), high-resolution P-wave data. The second field session used an orbital vibrator source that generates lower frequency (70–400 Hz), higher amplitude P- and S-waves, thereby allowing more spatial coverage (larger well spacings) and measurement of two rock properties, albeit with lower resolution than is available from the piezoelectric source data.

In this study, crosswell seismic data are used to infer the competency of basalt layers and the spatial distribution of "rubble" (highly fractured) zones. These zones, believed to be important to fracture flow and contaminant transport (Bukowski et al., 1998), are inferred from well logs, core sampling, and hydrologic testing. The seismic interpretations are compared with core and log data, where available. An understanding of the spatial distribution of fracturing is important for determining the scale at which the fractured aquifer can be numerically modeled as an equivalent porous medium. This determination is a current topic of research within the hydrologic community and at the TAN site (Bukowski and Sorenson, 1998). The scale information provided by seismic tomography proved valuable to the numerical modeling effort at INEEL (Bukowski and Sorenson, 1998).

SEISMIC CROSSWELL ANALYSIS IN FRACTURED, CRYSTALLINE AQUIFERS

Most crosswell seismic tomography has been performed in sedimentary formations important to oil and gas exploitation (Rector, 1995), and most laboratory studies of seismic properties use sedimentary rock (Mavko et al., 1998). However, aquifer contamination problems can occur in fractured crystalline rock, such as the Snake River Plain's basalt aquifer in Idaho. The application of crosswell seismic methods to fractured crystalline rock is often a more difficult problem, and it has been less studied than has the application to sedimentary rock.

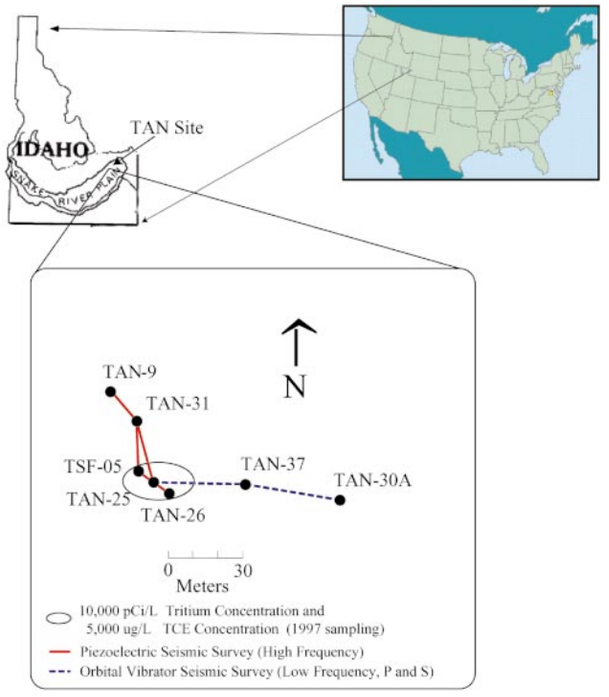

FIG. 1. Seismic tomography well locations at the INEEL TAN site in Idaho. Contaminant concentration contour is approximate; pCi/L = picocuries per liter. Snake River Plain from (Whitehead, 1992).

We know that fractures in rocks can cause large seismic velocity and amplitude changes compared with the intact matrix, and various approaches have been taken to develop a theory to relate seismic wave propagation to fracture properties (O'Connell and Budiansky, 1974; Hudson, 1981; Schoenberg and Sayers, 1995). Other subsurface features, such as matrix heterogeneity, fluid saturation, and partial gas saturation, make field measurement of fracture properties difficult in practice. Without attempting to directly invert for fracture properties, the seismic attributes can be related to subsurface features determined from other borehole methods (such as well pump tests, core analysis, and well logs). In this manner, crosswell imaging of seismic P-wave velocity and attenuation in fractured crystalline rock has been interpreted for the spatial distribution of fracture zones (Fehler and Pearson, 1984; Tura et al., 1992; Vasco et al., 1996). These studies show that low velocity and high attenuation of P-waves are observed in fracture zones, as models of seismic wave propagation in fractured rock predict.

Obtaining shear-wave information in addition to P-wave information can be very useful. Information about S-waves, especially the measurement of S-wave anisotropy, has been used to infer fracture properties (MacBeth and Lynn, 2000). In this study, generation of P- and S-waves by the orbital vibrator source allows direct measurement of the ratio V_p/V_s. This ratio, along with the related Poisson's ratio, is an important parameter in rock physics because, for a given density, V_s is controlled by the rock matrix's shear modulus, whereas V_p is controlled by both matrix and pore/fracture filling material (bulk and shear moduli). As V_p/V_s increases, the rock material properties are more of a "quasi-solid," with the limit being a fluid. Materials with open, fluid-filled fractures should tend to have a higher V_p/V_s. Most studies of V_p/V_s use core measurements for sedimentary rocks (see Mavko et al., 1998 for a review). Field measurement of V_p/V_s in altered, or nonsedimentary, fractured rock have generally been limited to VSP studies, (e.g., Daley et al., 1988; Pujol et al., 1989; Kuwahara et al., 1991), in which higher values are reported in fractured intervals.

The Committee on fracture characterization and fluid flow, U.S. national committee for rock mechanics (1996) gives an overview of seismic methods for detecting and delineating rock fractures.

In the following sections, we will describe the inversion approach, the field site, and crosswell data acquisition and processing (with separate treatments of the piezoelectric and orbital vibrator data sets). We will then present our interpretation of the two data sets separately, followed by our general conclusions.

INVERSION APPROACH

Estimating the spatial distribution of a seismic attribute between the wells used in crosswell acquisition requires a data inversion. The inversion used in this study is an algebraic reconstruction technique (ART) described by Peterson et al., (1985). This algorithm assumes straight raypaths between source and sensor locations. The cross-section between wells is divided

into square cells (0.5 m^2 for TAN data) and the seismic velocity is estimated in each cell. The relation between total travel time, t_k, and the 2D medium velocity, $\mathbf{V}(x, y)$, is given by

$$t_k = \int_{R_k} \frac{ds}{\mathbf{V}(x, y)} \tag{1}$$

for a segment s of the kth raypath R_k. Similarly, the seismic attenuation can be imaged by relating the seismic amplitude, A_k, to the 2D attenuation structure, $\alpha(x, y)$, through the equation

$$A_k = A_0 e^{[-\int_{R_k} \alpha(x,y)ds]}, \tag{2}$$

and the function P_k, where

$$P_k = ln\frac{A_k}{A_0} = -\int_{R_k} \alpha(x, y)ds \tag{3}$$

and where $\alpha(x, y) = \pi f/cQ$ for frequency f, velocity c, and attenuation factor Q. A_0 is the source amplitude corrected for radiation pattern, geometric spreading, and instrument response. In general, the problem is written

$$y_k = \int_{R_k} \mathbf{X}(r, s)ds, \tag{4}$$

with y_k representing the measured traveltime or amplitude for $k = 1, \ldots, N$ paths and $\mathbf{X}$ representing the slowness or attenuation operator. The problem is then discretized as a set of linear equations

$$y_k = \sum_{i=1}^{I} \delta_{ki} X_i \quad k = 1, \ldots, N \tag{5}$$

where δ_{ki} is the length of the ray k that penetrates pixel i, I is the total number of pixels intersected by the ray k, and X_i is the property of pixel i. The solutions are iterative and either require an initial velocity model or begin with simple backprojection of the data. The resolution of velocity in each cell is dependent on the seismic-ray density and weights that can be used to allow for varying ray length (Peterson et al., 1985).

One important factor that affects the accuracy of the inversion is determination of the relative depths and horizontal offsets of each source and receiver location (station). Errors in locations determined during acquisition can induce apparent static shifts in velocity for a given station. These errors can be the result of borehole deviation, which was measured incorrectly or not measured at all, and of survey errors in the borehole elevation. It is also important to correct for borehole effects, such as change in borehole diameter or mechanical properties of the rock immediately surrounding the borehole. Drilling-induced fracturing can alter rock properties as a function of depth, which will also provide a static shift in the measured traveltime for a given station. In the inversion used in this study, the traveltime data were simultaneously inverted for static shifts at each source and receiver station as well as for the velocity field as described in Vasco et al. (1996).

FIELD SITE DESCRIPTION AND CONTAMINANT CHARACTERIZATION

The geohydrologic framework of the Snake River Plain has been described by Whitehead (1992). The eastern plain is underlain by Quaternary-age basalt of the Snake River Group, with some sedimentary interbedding. The basalt section can be more than 1.5 km thick. The eastern plain has a sequence of thin-layered basalt flows, which can serve as significant aquifers. The TAN site of INEEL (Figure 1) overlies a portion of the eastern Snake River Plain's aquifer where the depth of the water table is about 60 m below ground level and basalt flows are interspersed with sedimentary interbeds.

A series of INEEL reports (Sorenson et al., 1996; Bukowski and Sorenson, 1998; Bukowski et al., 1998) describes the hydrologic flow conditions and contaminant distribution at TAN. From the water table down to the maximum drilled depth of about 98 m, the aquifer consists of numerous thin (1–6 m) basalt flows, with a thick flow below 100 m that limits downward migration. The aquifer is considered a multilayered aquifer system with high- and low-permeability layers. High-permeability layers are seen at the interface between individual basalt flows, which are described as fractured "rubble" zones. Thin sedimentary interbeds can act as relatively low-permeability aquitards. Figure 2 shows a conceptual model of the site, with hydrologic flow and barrier zones within the series of basalt flows. Groundwater sampling and straddle packer tests indicate stratification of flow within the aquifer (Bukowski et al., 1998).

The TAN site has mixed waste contamination, including the organics trichloroethylene (TCE), polychloroethylene (PCE) and dichloroethylene (DCE), along with radionuclides, which are believed to originate from a historic waste injection well (TSF-05 in Figure 1) (Sorenson et al., 1996). The plume is as much as 2 miles (3 km) long, with a "hot spot" shown in Figure 1. Gamma-log measurements in the boreholes give the most detailed estimates of contaminant distribution, particularly in the vertical direction. The gamma logs indicate the presence of gamma-emitting isotopes (e.g., cesium-137 and cobalt-60), which are believed to be entrained in the organic contaminant, and "it is assumed that TCE and other contaminants would follow the same preferential flow paths as Cs-137" (Sorenson et al., 1996). Gamma spectroscopy logging, performed in a subset of wells to identify man-made, gamma-emitting isotopes, has identified cesium-137 as the primary cause of gamma activity (Bukowski et al., 1998). Additional information about contaminant transport and distribution is given by TCE concentrations in core samples taken from well TAN-37. Borehole televiewer (BHTV) data were acquired in select wells, including only one of the seismic tomography wells, TAN-37. Borehole televiewer logs, which can image fractures at the borehole wall, were used to estimate the spatial distribution of fracture zones at TAN (Bukowski et al., 1998). Figure 3 shows gamma logs from tomography wells at the TAN site, along with core TCE concentration (Tobin et al., 2000) and BHTV data (both from well TAN-37).

Seismic imaging focused on the 60- to 90-m depth zone of the aquifer. The upper portion (approximately 60 to 75 m) of the seismic-tomography depth zone has two large gamma responses, seen most clearly in wells TAN-31, TAN-25, and TAN-26, at approximate depths of 66 and 72 m (Figure 3). The core TCE measurement from TAN-37 shows large concentrations from 66 to 70 m, 74 to 75 m, and 77 to 80 m. The BHTV log from TAN-37 shows multiple horizontal fractures (dark regions) between 70 and 80 m. These data and other well tests not reported here led the INEEL investigators to conclude that contaminant transport occurs mainly in horizontally stratified zones above about 100 m (Bukowski and

Sorenson, 1998; Bukowski et al., 1998). The seismic tomography was planned to aid in delineation of these zones.

TOMOGRAPHIC DATA ACQUISITION AND PROCESSING

High-frequency, piezoelectric-source acquisition

In November 1996, LBNL acquired seismic crosswell data at the TAN site, by use of a high-frequency (800–10,000 Hz) piezoelectric source designed at LBNL, along with commercial borehole hydrophone sensors. The source and sensors were stationed and data were collected, every 0.5 m, from just below the water table (approximately 65 m) to 100 m (or to the well bottom in shallower wells). Although high-quality piezoelectric data were obtained from five well pairs (Figure 1), limited propagation distance of the high frequency waves restricted the lateral extent of imaging. Other well pairs were attempted, but data usable for tomography were not obtained (Daley et al., 2001). The total seismic attenuation (including intrinsic and scattered losses) varied spatially. In general, the piezoelectric source could only propagate usable energy about 20 m between wells, with some zones having poor data at well spacings of 10–15 m. Usable energy is defined as that providing signal-to-noise ratios sufficient for first-arrival identification.

Figure 4 shows an example set of crosswell seismic recordings. The source is impulsive (similar to an explosive source) and the arrival time of the fastest seismic wave is picked at the point at which the waveform emerges from the background noise.

Prior to picking arrival times, the data processing consists of summing multiple shots of the source (typically about 25 shots) and bandpass filtering the broadband digital recordings to the frequency band of the seismic energy (typically 800 to 8000 Hz).

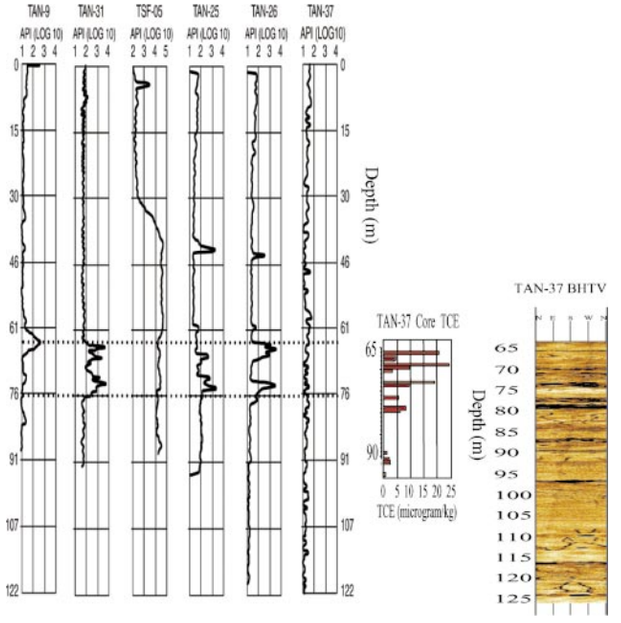

FIG. 3. Example wellbore data used for site characterization and seismic tomography interpretation: gamma logs (six on left), core TCE concentration (second from right), and borehole televiewer amplitude (right). Data are from tomography wells whose locations are shown in Figure 1. High gamma counts correlated between wells (dashed lines) indicate zones of contaminant transport within the aquifer (Bukowski and Sorenson, 1998). Note the higher scale values for the TSF-05 gamma log, which was the presumed historic injection well for contaminant disposal. Dark regions (less reflection amplitude) in televiewer amplitude data are interpreted to be fractures or fracture zones.

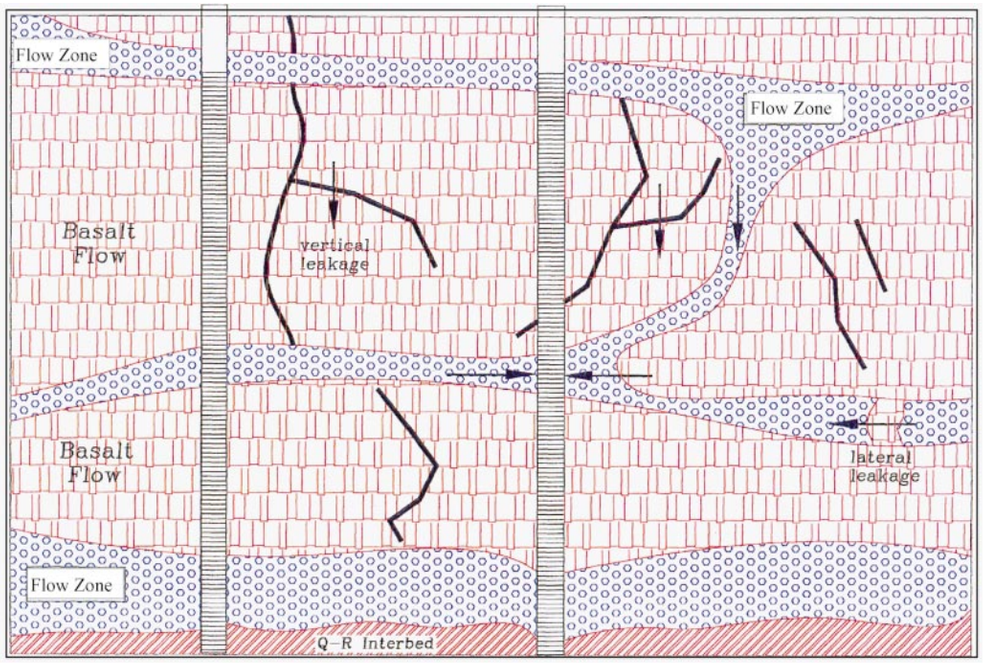

FIG. 2. Conceptual model of hydrologic flow within the aquifer at the INEEL TAN site (modified from Bukowski et al (1998). Interbed fractured rubble zones are believed to be high-permeability zones (labeled "Flow Zone"). Sedimentary interbeds (e.g., Q-R) can act as a relatively low-permeability barrier to vertical flow.

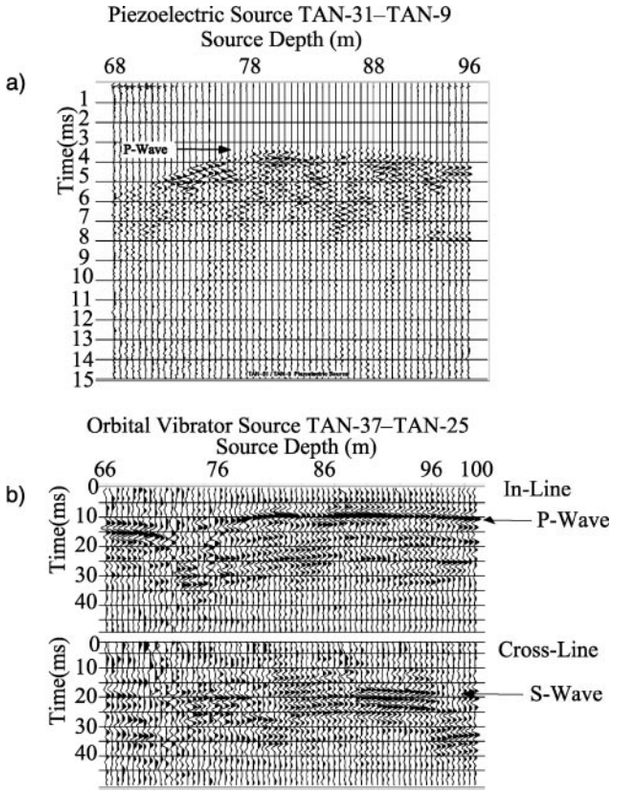

FIG. 4. Seismograms sorted into receiver gathers for the piezoelectric (a) and orbital vibrator (b) seismic sources. For both examples, the receiver depth is 85 m and the source depths are 66 to 100 m. The orbital vibrator data (b) contain separate in-line and cross-line source components of motion, which generate predominantly P-wave and S-wave energy, respectively.

After we picked the arrival times, we made various checks on the quality and consistency of picks, including analyzing traveltime versus distance and traveltime versus source-receiver offset. Times found to be in error (mispicked) are repicked or removed from the traveltime data set, whereas the remaining traveltimes are used for tomographic inversion, as previously described in equations (1) through (5). Figure 5 shows the inversion results for piezoelectric source data.

The TAN-31 and TAN-9 data set has also been inverted for seismic attenuation using the amplitude of the first arrival, within a constant-length time window, computed for each seismic trace that had sufficient signal-to-noise ratio. The cross-section between wells was then divided into pixels, and each pixel was inverted for amplitude attenuation α in dB/m. Whereas seismic amplitudes are affected by many factors, including the velocity structure and elastic impedance contrast at the borehole, they have shown a relationship with permeable fracture zones in a fractured aquifer (Vasco et al., 1996). Figure 6 shows the attenuation inversion result for TAN-31 and Tan-9 data, along with velocity and gamma log data.

Orbital vibrator source acquisition of P- and S-waves

A new well, TAN-37, was drilled at the TAN site in 1997. The crosswell distances to this well were too long to acquire piezoelectric source data (based on total seismic attenuation seen in the previous surveys). The desire to image from the existing wells to this new well led us to consider the use of the orbital-vibrator (OV) source, which has higher energy output and lower frequency content than does the piezoelectric source. The OV is a swept-frequency borehole seismic source designed for oil and gas exploration (Daley and Cox, 2001). A DC-powered version of the orbital vibrator runs on a standard 7-conductor armored cable. The OV also has the notable

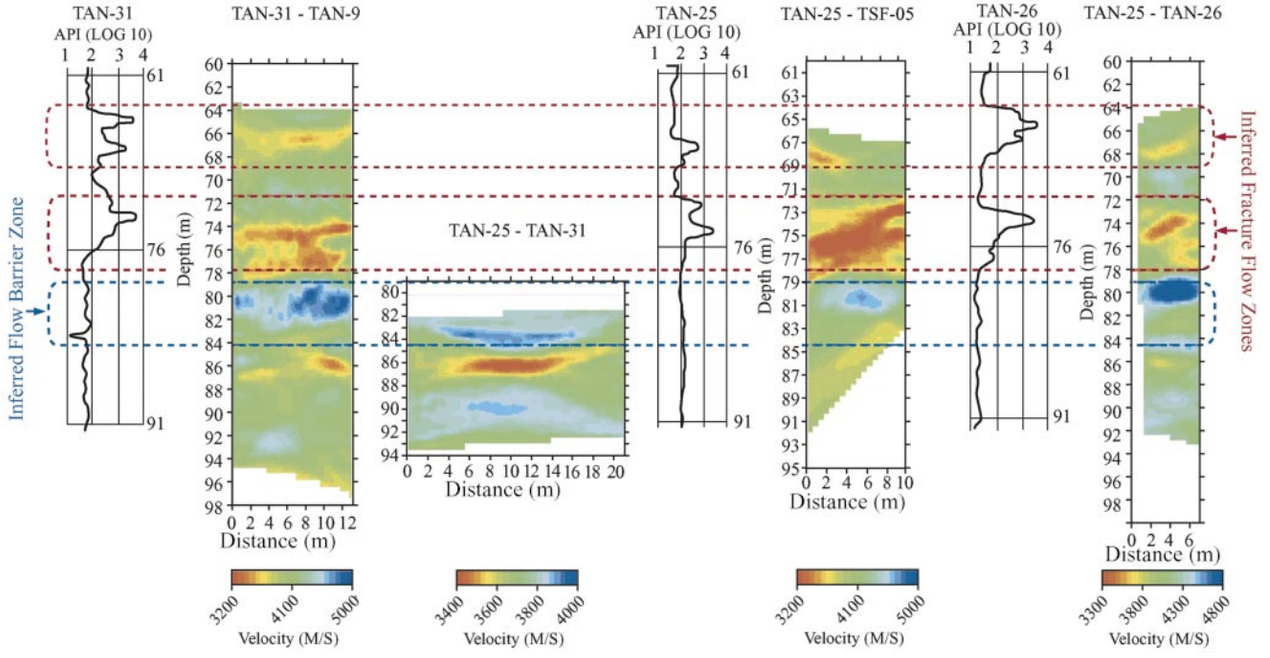

FIG. 5. Seismic velocity tomograms from the INEEL TAN site with select gamma logs from Figure 3. Zones of low velocity (yellow-red) are interpreted to be fractured basalt that allows contaminant transport within the aquifer. High velocity zones (blue), such as the zone at 80–84 m, are interpreted to be dense, unfractured basalt zones that act as a barrier to contaminant flow within the aquifer.

advantage of generating P- and S-wave energy simultaneously. Additionally, although the lower frequency content (70 to 400 Hz) yields lower spatial resolution, it also increases the propagation distance in material of a given attenuation. Tests at the TAN site during OV acquisition showed we could acquire data over the 57 m between wells TAN-37 and TAN-31. At this distance, the survey aperture (ratio of available well depth to well separation) becomes the limiting factor, because decreasing the aperture results in degradation of tomographic resolution (Peterson et al., 1985).

Orbital-vibrator data were successfully acquired in two well pairs using TAN-37 as a source borehole (Figure 1), thereby extending the range of crosswell seismic surveys in the fractured basalt aquifer of the TAN site. Figure 4b shows typical recordings from the TAN-37 and TAN-25 well pair, where the well separation was 38 m.

The OV acquisition also proved successful in acquiring P- and S-wave data using fluid-coupled hydrophone sensors. This represents the first use of hydrophone sensors with an orbital vibrator (Daley and Cox, 2001) and demonstrates a more economical survey technique, because hydrophones typically have more sensors per cable and faster acquisition than clamping borehole geophones. Therefore, data acquisition within aquifers is very efficient because the OV source is also fluid coupled (with no clamping required). The relatively high amplitude of S-waves generated by the OV (see Figure 4b) can overcome reduced shear-wave sensitivity of hydrophones, which sense the fluid-pressure pulse converted from incident S-waves, as compared with wall-locking sensors, which directly measure the shear motion of S-waves. The acquisition of an S-wave crosswell survey, in addition to the standard P-wave survey, offers additional information about subsurface material properties.

Orbital vibrator processing

The orbital-vibrator seismic source requires a unique pre-inversion processing sequence, including source signal deconvolution and vector decomposition (Daley and Cox, 2001). This processing yields two data sets containing source energy in the plane of the boreholes and energy normal to that plane (labeled in-line and cross-line in Figure 4b). These data have separation of the P- and S-waves (where the S-wave has a horizontal polarization for a vertical borehole). Both the P- and S-wave traveltimes are picked and analyzed with the method described in equations (1) through (5). Figure 7 shows the P- and S-wave tomograms obtained from tomographic inversion of the OV data for wells TAN-37 and TAN-25.

The OV data for wells TAN-37 and TAN-30a were processed identically to the data from wells TAN-37 and TAN-25. However, there was a strong tube wave recorded in well TAN-30a. A tube wave is a type of interface wave at the borehole wall in fluid-filled boreholes (White, 1965). We did not analyze the S-wave traveltime picks for the TAN-37 and TAN-30a well pair because of the tube-wave noise in well TAN-30a.

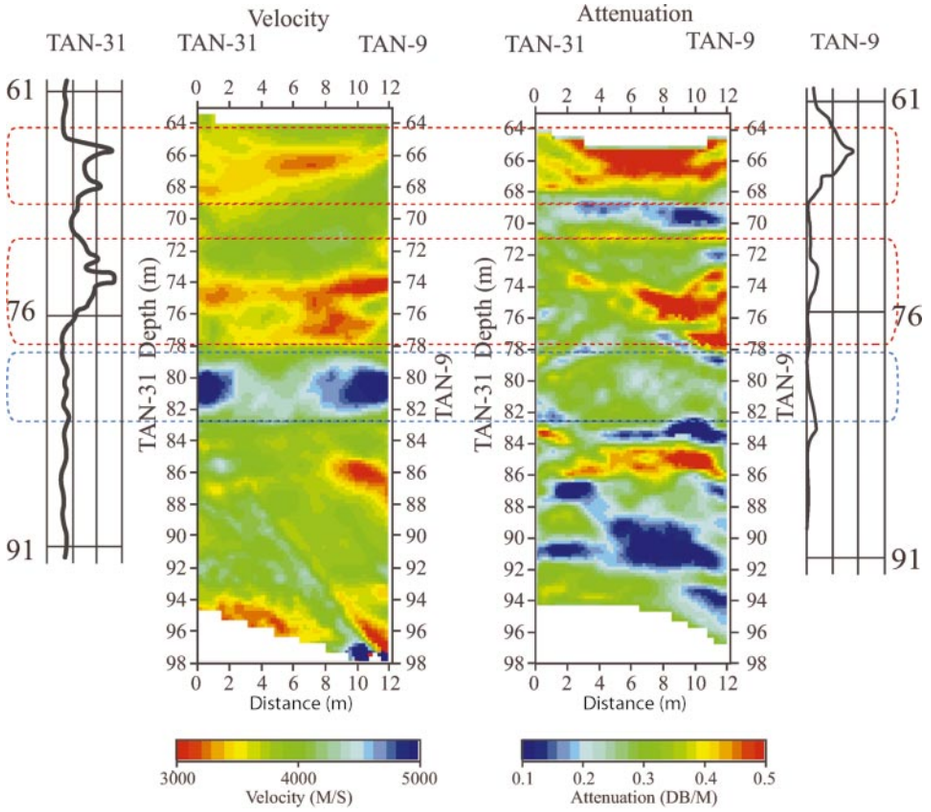

FIG. 6. Seismic velocity and attenuation results for well pair TAN-31 and TAN-9, along with gamma logs from the same wells.

The two P-wave OV tomograms form an image spanning wells TAN-25 to TAN-37 to TAN-30a (Figure 1). These two P-wave tomograms are shown in Figure 8, along with the borehole televiewer log from well TAN-37.

INTERPRETATION

Piezoelectric data

High-quality P-wave arrivals were obtained with the piezoelectric seismic source at the TAN site, over much of the 65- to 100-m survey depths. Seismic attenuation limited data quality in some depth zones. The traveltime measurements were used to generate five crosswell tomograms, four of which are in the contaminant "hot spot" and are shown in Figure 5. During inspection of data gathers (e.g., Figures 4a and 4b), coherent reflections, which might indicate sedimentary interbeds in the depth range of the survey, were not observed. Additionally, Figure 6 (the attenuation and velocity tomograms for the TAN-31 and TAN-9 well pair) shows low velocity associated with high attenuation, which indicates fracturing (Vasco et al., 1996). The observed velocity variations are therefore interpreted as fracture-induced material property variations of the basalt flows, not sediment-basalt interbedding.

The four tomograms shown in Figure 5 reveal laterally consistent patterns of seismic velocity. In Figure 5, three distinct and spatially persistent depth zones are interpreted; two low-velocity zones are interpreted as fractured (high-flow) zones, and one high-velocity zone is interpreted as a less fractured (flow-barrier) zone. This interpretation is based on previous field observations (Tura et al., 1992; Vasco et al., 1996) and on the theory (e.g., Hudson, 1981, Pyrak-Nolte et al., 1990; Schoenberg and Sayers, 1995) that velocity is affected by fracturing, with higher velocity corresponding to competent, less fractured rock. Furthermore, fracture flow models indicate that, as the rock fracture density increases, fracture connectivity increases and permeability can increase (Committee on fracture characterization and fluid flow, U.S., national committee for rock mechanics, 1996).

The predominantly horizontal stratification revealed by the tomograms is interpreted to be imaging independent basalt flows, with low velocity as a result of fracturing in the flow boundary region and high velocity occurring in the less fractured inner-flow region. In Figures 5 and 6, the upper two (64–69 m and 72–78 m) low-velocity zones are interpreted to be interflow fracture/rubble zones with higher flow and transport. The high-velocity zone from about 79 to 84 m is interpreted to be a more intact basalt zone that acts as a barrier to vertical flow and therefore preventing significant contaminant migration from the upper section. This interpretation is supported by other well test results (Bukowski et al., 1998).

The TAN-25 and TAN-31 data had very high apparent attenuation in the upper section (above 80 m), thereby causing very poor data quality, which prevented traveltime picking and tomographic analysis (note the blank upper section of the tomogram in Figure 5). High apparent attenuation can be caused by increased fracture content, borehole effects, and also by high TCE [or other dense nonaqueous phase liquid (DNAPL)] concentration (Geller and Myer, 1995) and increased partial gas saturation (Mavko et al., 1998). Borehole effects can be ruled out as the cause of this high attenuation, because both wells TAN-25 and TAN-31 were used for other tomograms that had higher velocity and lower attenuation. The variation in data quality observed in this well pair suggests that contaminant effects, such as DNAPL content or gas generation, may have an effect on attenuation.

In general, the features on the piezoelectric tomograms can be interpreted for interfaces and features to about a 1 to 2-m resolution. These interpretations on the 1-m scale are considered to be the spatial limit of interpretability. Lateral resolution generally is not as good as is the vertical resolution (Peterson

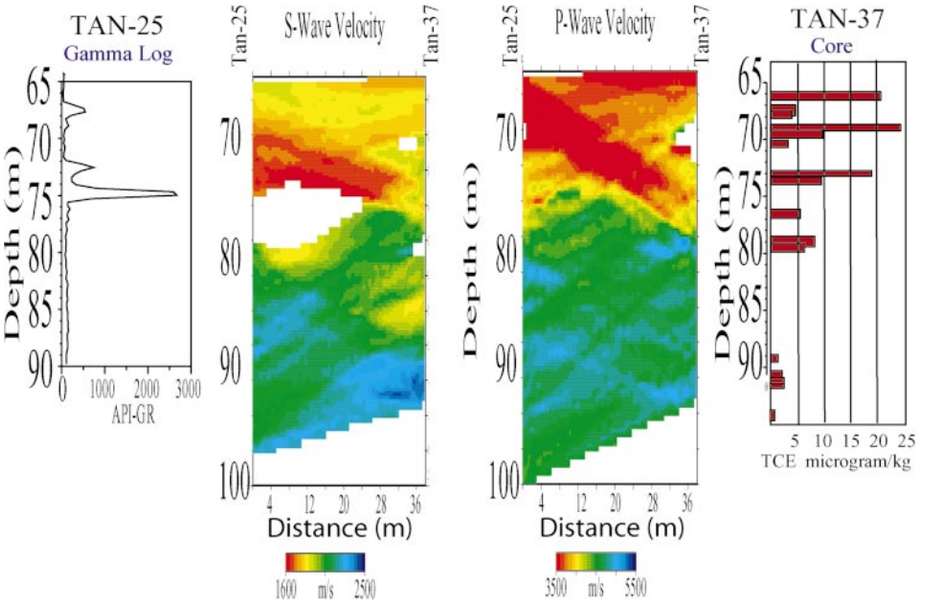

FIG. 7. Comparison of orbital vibrator crosswell velocity tomograms, with core contaminant sampling and gamma log.

et al., 1985), so lateral variations within horizons between wells are less resolved and are not interpreted.

Orbital-vibrator data

The lower frequency content of the orbital vibrator source, along with the larger interwell distances acquired with the OV, leads to lower resolution imaging of the subsurface velocity structures. Figure 7 shows the P- and S-wave tomograms for TAN-25 and TAN-37, whereas Figure 8 shows the two P-wave tomograms along with the borehole televiewer data from TAN-37. The upper two low-velocity zones (spanning 64 to 78 m) identified with the piezoelectric source data are imaged as one zone (with some separation in the TAN-37 and TAN-30a tomogram). Figure 7 shows the gamma logs for well TAN-25 and core samples of TCE concentrations from well TAN-37, along with the crosswell tomograms. The gamma logs and the core samples confirm the presence of contaminant transport zones between 65 and 80 m. The borehole televiewer data show distinct horizontal fractures (dark regions) at about 74 and 77–79 m. We interpret the seismic low-velocity zone of about 65 to 78 m to be fractured basalt. The deeper low-velocity zone (at about 86–88 m) on the piezoelectric tomograms is not imaged in the OV tomograms.

V_p/V_s values were calculated from the TAN-25 and TAN-37 P- and S-wave tomography. Taking simple ratios of the tomogram data did not provide a spatially coherent image (Daley et al., 2001), but a V_p/V_s range was found. The V_p/V_s values range from below 1.8 to over 2.8, which are high values compared with a typical Poisson solid ($V_p/V_s = 1.73$) and laboratory measurements of intact basalt where $V_p/V_s = 1.74$ (Carmichael, 1982), and VSP measurement of Columbia Plateau basalt $V_p/V_s = 2$ (Pujol et al., 1989). These high V_p/V_s values concur with other evidence of fracturing of the basalt.

The resolution obtained with the lower frequency OV data is worse than with the piezoelectric source. However, the dominant feature of low velocities in the upper aquifer between 65 and 78 m (Figure 8) is well delineated in both tomograms and coincides with the location of two fracture zones identified using the piezoelectric data (Figure 5). Whereas the issue of the correct scale of equivalent porous media modeling cannot be addressed by seismic imaging alone, the scale of such modeling chosen for the TAN site is adequately constrained by the lower resolution orbital vibrator data [J. Bukowski, personal communication, 1999].

An OV test recording between wells TAN-37 and TAN-31 (Figure 1) showed usable arrivals at a distance of 57 m. Thus, the subsurface heterogeneity that impacts the hydrologic models can be detected by seismic tomography at these distances.

SUMMARY AND CONCLUSIONS

At a fractured basalt aquifer within the INEEL TAN site, multiple high-frequency P-wave data sets in close well spacings (less than 25 m) were acquired with a piezoelectric seismic source. An orbital vibrator seismic source was also used to acquire P- and S-wave data sets in larger well spacings (nearly 40 m), with P-waves recorded at nearly 60-m well spacing. The use of the OV with a hydrophone array successfully demonstrated the applicability of this new type of seismic source for environmental applications needing both P- and S-wave measurements. Traveltime tomography was performed for both P- and S-wave data sets. The P-wave velocities ranged from less than 3200 m/s to greater than 5000 m/s. The success of the initial piezoelectric source tomograms in defining thin zones with about 1- to 2-m resolution in the upper high-flow section was limited by the distances between wells that could be surveyed because of attenuation of the seismic signal. The follow-up survey, performed using the orbital vibrator (a more powerful, lower frequency seismic source), resolved the upper high-flow section as a 10- to 15-m thick unit over larger distances between wells.

The combination of well logs, core samples, and crosswell imaging spans many scale lengths for estimating subsurface properties. Using the V_p, V_s, and attenuation tomograms, together with gamma-ray, borehole televiewer, and TCE concentration in core samples, we interpreted the tomograms for intact versus fractured zones, assuming that high apparent contaminant transport occurs in the fractured zones. The 10- to 15-m resolution of the OV data is consistent with the scale used for hydrologic modeling of the TAN site as an equivalent, porous medium (Bukowski et al., 1998). This consistency is important because the OV's lower frequency content, coupled with higher output energy, leads to imaging over larger distances. The higher resolution of the piezoelectric tomograms is not necessary for the large-scale hydrologic modeling currently used for remediation at the TAN site. The higher resolution piezoelectric data were used to confirm conceptual models of the aquifer.

From the P- and S-wave tomograms, the ratio V_p/V_s was calculated, with values ranging from 1.8 to 2.8. The direct subsurface measurement of this ratio is useful for understanding material properties. Future work with OV crosswell data could lead to tomographic imaging of V_p/V_s.

In general, at the fractured basalt TAN site, regions of slow seismic velocity are found to correspond with zones of contamination (and, by inference, higher transport and increased

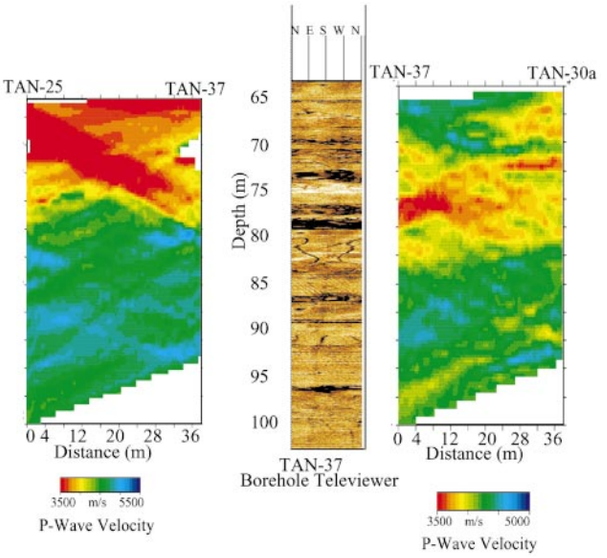

FIG. 8. TAN site P-wave orbital vibrator seismic tomography (wells TAN-25 and TAN-37 left; wells TAN-37 and TAN-30a right), along with borehole televiewer (center).

fracturing). Regions of low amplitude (high attenuation) also appear to correspond with zones of high contaminant transport. Regions of anomalously high attenuation, such that tomography could not be achieved between certain wells, suggest that other factors, such as DNAPL concentration or partial gas saturation, may be affecting wave propagation at the TAN site.

The combination of piezoelectric data for closer well spacing and orbital vibrator data for larger well spacings has provided optimal imaging capability and has been instrumental in understanding the TAN site aquifer's hydrologic properties and its scale of heterogeneity.

ACKNOWLEDGMENTS

This work was supported by the Environmental Management Science Program (EMSP) of the U.S. Department of Energy, under contract no. DE-AC03-76SF000098. Data processing was performed at the Center for Computational Seismology, which is supported by the Director, Office of Energy Research, Office of Basic Energy Sciences, of the U.S. Department of Energy under contract No. DE-AC03-76SF000098. Assistance at INEEL was provided by Tom Wood, Chad Hersley, and Rick Colwell. Special thanks go to John Bukowski, formerly of INEEL, for discussions of the hydrologic conceptual and numerical modeling. The authors would like to thank Tom Wood of INEEL and Ken Williams and Don Lippert of LBNL for assisting data acquisition during a cold Idaho winter. Several reviewers contributed to improving the original manuscript.

REFERENCES

Bukowski, J. M., Bullock, H., and Neher, E. R., 1998, Site conceptual model: 1997 activities, data analysis, and interpretation for test area north, operable unit 1-07B: Idaho National Engineering and Environmental Laboratory report INEEL/EXT-98-00575.

Bukowski, J. M., and Sorenson Jr., K. S., 1998, Site conceptual model: 1996 activities, data analysis, and interpretation for test area north, operable unit 1-07B: Idaho National Engineering and Environmental Laboratory Report INEEL/EXT-97-00556.

Cao, S., and Greenhalgh, S., 1997, Cross-well seismic tomographic delineation of mineralization in a hard rock environment: Geophysical Prospecting, **45**, 449–460.

Carmichael, ed., 1982, Handbook of physical properties of rocks volume II: CRC Press, Inc.

Committee on fracture characterization and fluid flow, U.S. national committee for rock mechanics, 1996, Rock fractures and fluid flow: Contemporary understanding and applications: National Academy Press, 167–242.

Daley, T. M., McEvilly, T. V., and Majer, E. L., 1988, Analysis of P and S wave vertical seismic profile data from the Salton Sea scientific drilling project: Journal of Geophysical Research, **93**, 13,025–13,026.

Daley, T. M., Majer, E. L., and Peterson, J. E., 2001, Crosswell seismic imaging in a contaminated basalt aquifer—final report: Lawrence Berkeley National Laboratory Report, LBNL-45533, Berkeley, Ca.

Daley, T. M., and Cox, D., 2001, Orbital vibrator seismic source for simultaneous P- and S-wave crosswell acquisition: Geophysics, **66**, 1471–1480.

Fehler, M., and Pearson, C., 1984, Cross-hole seismic surveys: Applications for studying subsurface fracture systems at a hot dry rock geothermal site: Geophysics, **49**, 37–45.

Geller, J. T., and Myer, L. R., 1995, Ultrasonic imaging of organic liquid contaminants in unconsolidated porous media: Journal of Contaminant Hydrology, **19**, 85–104.

Harris, J. M., Nolen-Hoeksema, R. C., Langan, R. T., Van Schaack, M., Lazaratos, S. K., and Rector, J. W. III, 1995, High-resolution cross-well imaging of a west Texas carbonate reservoir: Part 1—Project summary and interpretation: Geophysics, **60**, 667–681.

Hubbard, S. S., Rubin, Y., and Majer, E., 1999, Spatial correlation structure estimation using geophysical and hydrogeological data: Water Resources Research, **35**, **6**, 1809–1825.

Hudson, J. A., 1981, Wave speeds and attenuation of elastic waves in material containing cracks: Geophysical Journal of the Royal Astronomical Society, **64**, 133–150.

Hyndman, D. W., Harris, J. W., and Gorelick, S. M., 1994, Coupled seismic and tracer test inversion for aquifer property characterization: Water Resources Research, **30**, 1965–1977.

Hyndman, D. W., and Gorelick, S. M., 1996, Estimating lithologic and transport properties in three dimensions using seismic and tracer data: The Kesterson aquifer: Water Resources Research, **32**, 2659–2670.

Kuwahara, Y., Ito, H., and Kiguchi, T., 1991, Comparison between natural fractures and fracture parameters derived from VSP: Geophysical Journal International, **107**, 475–483.

MacBeth, C., and Lynn, H. B., eds., 2000, Applied seismic anisotropy: Theory, background and field studies: Geophysics Reprint Series, Society of Exploration Geophysicists.

Mason, I. M., 1981, Algebraic reconstruction of a two-dimensional velocity inhomogeneity in the High Hazles seam of Thoresby colliery: Geophysics, **46**, 298.

McKenna, S. A., and Poeter, E. P., 1995, Field example of data fusion in site characterization: Water Resources Research, **31**, 3229–3240.

Mavko, G., Mukerji, T., and Dvorkin, J., 1998, The rock physics handbook: Cambridge University Press.

O'Connell, R. J., and Budiansky, B., 1974, Seismic velocities in dry and saturated cracked solids: Journal of Geophysical Research, **79**, 5412–5426.

Peterson, J. E., Paulsson, B. N. P., and McEvilly, T. V., 1985, Applications of algebraic reconstruction techniques to crosshole seismic data: Geophysics, **50**, 1566–1580.

Pujol, J., Fuller, B. N., and Smithson, S. B., 1989, Interpretation of a vertical seismic profile conducted in the Columbia Plateau basalts: Geophysics, **54**, 1258–1266.

Pyrak-Nolte, L. J., Myer, L. R., and Cook, N. G. W, 1990, Anisotropy in seismic velocities and amplitudes from multiple parallel fractures: Journal of Geophysical Research, **95**, 11345–11358.

Rector, J. W. III, ed., 1995, Special issue: Crosswell methods: Geophysics, **60**, 629–630.

Rector, J. W. III, Lazaratos, S. K., Harris, J. M., and Van Schaack, M, 1995, High-resolution crosswell imaging of a west Texas carbonate reservoir: Part 3—Wavefield separation of reflections: Geophysics, **60**, 692–701.

Rubin, Y., Mavko, G., and Harris, J., 1992, Mapping permeability in heterogeneous aquifers using hydrologic and seismic data: Water Resources Research, **28**, 1809–1816.

Schoenberg, M., and Sayers, C. M., 1995, Seismic anisotropy of fractured rock: Geophysics, **60**, 204–211.

Sorenson Jr., K. S., Wylie, A. H., Wood, T. R., 1996, Test area north site conceptual model and proposed hydrogeologic studies, operable unit 1-07B: Idaho National Engineering Laboratory report INEL-96/0105.

Tobin, K. J., Colwell, F. S., Onstott, T. C., and Smith, R., 2000, Recent calcite spar in an aquifer waste plume: a possible example of contamination driven calcite precipitation: Chemical Geology **169**, 449–460.

Tura, M. A. C., Johnson, L. R., Majer, E. L., and Peterson, J. E., 1992, Application of diffraction tomography to fracture detection, Geophysics: **57**, 245–257.

Vasco, D. W., Peterson, J. E., and Majer, E. L., 1996, A simultaneous inversion of seismic travel times and amplitudes for velocity and attenuation: Geophysics, **61**, 1738–1757.

White, J. E., 1965, Seismic waves: radiation, transmission, attenuation: McGraw Hill, Inc.

Whitehead, R. L., 1992, Geohydrologic framework of the snake river plain regional aquifer system, Idaho and eastern Oregon: U.S. Geological Survey Professional Paper 1408-B.

Yamamoto, T., Nye, T., and Kuru, M., 1995, Imaging the permeability structure of a limestone aquifer by crosswell acoustic tomography: Geophysics, **60**, 1634–1645.